

## Detecting natural influence on surface air temperature change in the early twentieth century

Toru Nozawa,<sup>1</sup> Tatsuya Nagashima,<sup>1</sup> Hideo Shiogama,<sup>1</sup> and Simon A. Crooks<sup>2</sup>

Received 18 May 2005; revised 6 September 2005; accepted 23 September 2005; published 29 October 2005.

[1] We analyze surface air temperature datasets simulated by a coupled climate model forced with different external forcings, to diagnose the relative importance of these forcings to the observed warming in the early 20th century. The geographical distribution of linear temperature trends in the simulations forced only by natural contributions (volcanic eruptions and solar variability) shows better agreement with observed trends than that does the simulations forced only by well-mixed greenhouse gases. Using an optimal fingerprinting technique we robustly detect a significant natural contribution to the early 20th century warming. In addition, the amplitude of our simulated natural signal is consistent with the observations. Over the same period, however, we could not detect a greenhouse gas signal in the observed surface temperature in the presence of the external natural forcings. Hence our analysis suggests that external natural factors caused more warming in the early 20th century than anthropogenic factors. **Citation:** Nozawa, T., T. Nagashima, H. Shiogama, and S. A. Crooks (2005), Detecting natural influence on surface air temperature change in the early twentieth century, *Geophys. Res. Lett.*, 32, L20719, doi:10.1029/2005GL023540.

### 1. Introduction

[2] According to recent detection and attribution studies [e.g., *Mitchell et al.*, 2001], it is extremely likely that the global warming observed over the last three decades is attributed to human influences, primarily to an increase in concentrations of well-mixed greenhouse gases (WMGHGs). However, there is considerable uncertainty about the surface air temperature (SAT) response in the early 20th century. Possible causes include greenhouse-gas induced warming [*Tett et al.*, 1999, 2002, hereinafter referred to as T02; *Stott et al.*, 2001; *Hegerl et al.*, 2003], internal variability [*Delworth and Knutson*, 2000], and natural climate forcings [*Broccoli et al.*, 2003; *Meehl et al.*, 2004]. While *Broccoli et al.* [2003] also suggested that the early-century warming could arise from a combined effect of the internal variability and the natural forcings, T02 and *Hegerl et al.* [2003] mentioned that the early warming could stem from a combined effect of the WMGHGs and the natural contributions. Therefore, owing to this obvious lack of agreement, we feel further inves-

tigations are required to clarify which forcing factors contribute greatly to the early 20th century warming.

[3] In this study, we compare simulated SATs from a global coupled ocean-atmosphere general circulation model (CGCM) to an observed SAT dataset [*Jones and Moberg*, 2003]. In particular, these simulations are used to estimate the natural and anthropogenic contributions to the observed temperature increase in the early 20th century. To minimize the uncertainty that arises from missing external forcing factors, all the known major natural and anthropogenic forcings are included in our model simulations, although, as in all historical simulations, inevitable uncertainties in the included forcings remain. An optimal fingerprinting method [*Hasselmann*, 1997; *Allen and Stott*, 2003] is applied in order to detect natural and/or anthropogenic influences on the early SAT increase.

### 2. Model and Experiments

[4] We used a coupled climate model generally known as MIROC [*Hasumi and Emori*, 2004], which is a CGCM collaboratively developed by the Center for Climate System Research of the University of Tokyo (CCSR), the National Institute for Environmental Studies (NIES), and the Frontier Research Center for Global Change of the Japan Agency for Marine-Earth Science and Technology (FRCGC). In the atmosphere it has a spatial resolution of T42L20, while in the ocean it has 1.4° (longitude) by variable 0.56–1.4° (latitude) in the horizontal and 44 levels in the vertical. No flux correction is applied in exchanging heat, water, and momentum flux between the atmosphere and the ocean. Our model represents radiative effects of CO<sub>2</sub>, CH<sub>4</sub>, N<sub>2</sub>O, and sixteen species of (H)(C)FCs individually [*Nakajima et al.*, 2000]. The atmospheric component of MIROC has an interactive aerosol transport module [*Takemura et al.*, 2002] which can handle major tropospheric aerosols (sulfate, black carbon, organic carbon, sea salt, and soil dust). It also includes an explicit representation of the first and second kinds of indirect effects induced by soluble aerosols, as well as the direct effects of all aerosols. The equilibrium climate sensitivity to a doubling of CO<sub>2</sub> concentrations of the atmospheric part of MIROC coupled to a mixed-layer ocean is 4.0K in this resolution.

[5] Four ensembles with different combinations of external forcing factors were carried out for the period from 1850 to 2000. The first one is FULL, where the simulations were forced with both natural and anthropogenic forcings: changes in solar irradiance [*Lean et al.*, 1995], stratospheric volcanic aerosols [*Sato et al.*, 1993], WMGHGs [*Johns et al.*, 2003], tropospheric and stratospheric ozone [*Sudo et al.*, 2002; *Randel and Wu*, 1999], surface emissions of anthropogenic carbonaceous aerosols (T. Nozawa and

<sup>1</sup>National Institute for Environmental Studies, Tsukuba, Japan.

<sup>2</sup>Department of Physics, University of Oxford, Oxford, UK.

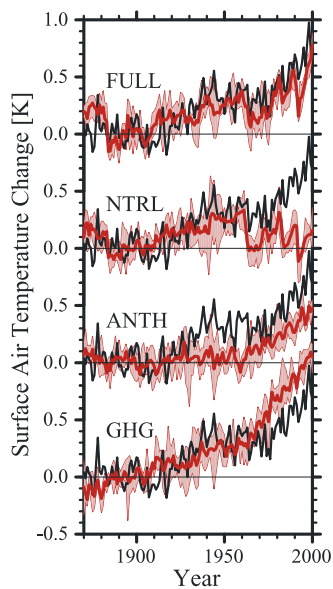


**Figure 1.** Temporal variations of global annual mean surface air temperature (SAT). Anomalies from the 1881–1910 mean for the observations [Jones and Moberg, 2003] (thick black line) and the ensemble mean of the FULL, NTRL, ANTH, and GHG simulations (thick red lines). Maximum and minimum ranges from the individual simulations are shaded in light red. In calculating the global annual mean SAT, modeled data are projected onto the same resolution of the observations discarding simulated data at grid points where there was missing observational data. More than ten months of data were required at each location to calculate the annual mean value.

J. Kurokawa, Historical and future emissions of sulfur dioxide and black carbon for global and regional climate change studies, manuscript in preparation, 2005) and precursors of sulfate aerosols [Lefohn *et al.*, 1999] and land-use [Hirabayashi *et al.*, 2005]. The second is NTRL and the third is ANTH, where the simulations were forced with

the natural and the anthropogenic forcings, respectively. The final ensemble is GHG, where the simulations were forced with changes in WMGHGs only. Each ensemble consists of four ensemble simulations starting from different initial conditions taken from a pre-industrial control run.

[6] The pre-industrial control run is performed for 1300 years after a 200-year spin up simulation. The control run shows no significant climate drift; linear trend in the global annual mean SAT is no more than 0.02K/century. In addition, simulated decadal variability of the control run is comparable to the decadal variability found in observations. For example, the standard deviation of the observed global decadal mean SAT, calculated from linearly detrended data for the 1900–1949 period, falls within the minimum and maximum range of the simulated standard deviations for 50-year segments of the control run. An F-test reveals that there is no significant disagreement between the observed and the modeled decadal variability.

### 3. Results

[7] Figure 1 shows temporal variations of the global annual mean SAT for the FULL, NTRL, ANTH, and GHG ensembles. The observed SAT is superposed on each ensemble. The FULL ensemble captures well the observed multi-decadal variations throughout the 20th century. In all ensembles except for NTRL, simulated SATs show remarkable temperature increase after 1970s in close agreement with observed temperatures, suggesting that the observed warming in the recent three decades resulted primarily from an increase in concentrations of WMGHGs. On the other hand, all ensembles other than ANTH capture the early-century warming. In the ANTH simulations, the warming due to WMGHGs is offset by a cooling due to increases in anthropogenic aerosols, resulting in no significant warming until 1950s (T. Nagashima *et al.*, Effect of carbonaceous aerosols on the surface temperature in the mid 20th century, submitted to Geophysical Research Letters, 2005). The simulated temperature increase in NTRL in the first half of the 20th century is about 0.5K/century, which is slightly less than that in the observations. This global annual mean

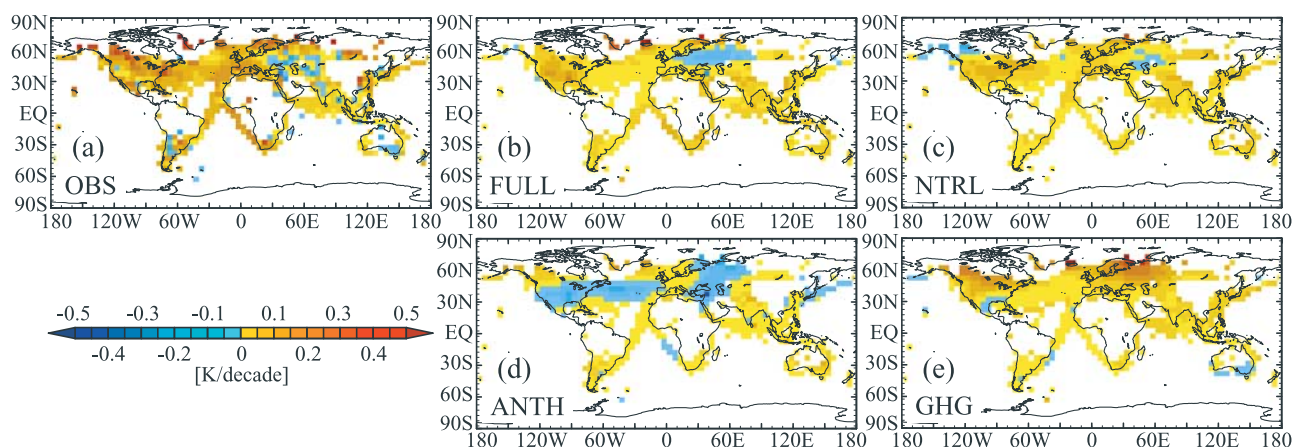


**Figure 2.** Geographical distributions of linear SAT trends (K/decade) in the first half of the century for the (a) observations [Jones and Moberg, 2003] and the ensemble means of the (b) FULL, (c) NTRL, (d) ANTH, and (e) GHG simulations. Trends were calculated from annual mean values only for those grids where the annual data is available in at least 2/3 of the 50 years and distributed in time without significant bias.

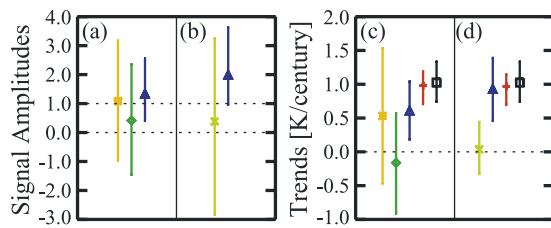


**Figure 3.** Best-estimated (a, b) signal amplitudes and (c, d) linear trends (K/century) with 5–95% uncertainty ranges for the 50-year segment from 1900 to 1949 for the GHG, ANTH-GHG (anthropogenic signal other than WMGHGs) (Figures 3a and 3c), and the NTRL analysis and for the ANTH and NTRL analysis (Figures 3b and 3d). The orange error bar with an asterisk, green error bar with a diamond, light green error bar with a cross, and blue error bar with a triangle indicates GHG, ANTH-GHG, ANTH, and NTRL, respectively. Also shown in Figures 3c and 3d are the total reconstructed trend in the regression model (red error bar with a plus) and the observed (solid error bar with a square) trend. Error bars denote 5–95% uncertainty ranges.

SAT trend in NTRL is larger than that of *Stott et al.* [2000] and T02 ( $\sim 0.3\text{K/century}$ ) for their simulations with natural forcings only, although we use identical natural forcing datasets to the ones they used. The trend of the global annual mean SAT in GHG is nearly equal to that in NTRL; therefore, without further investigation, we cannot conclude which factors are the main contributors to the observed early warming.

[8] Geographical distributions of linear SAT trends for the first half of the century are shown in Figure 2 for the observations and the ensemble mean of each ensemble. The trend patterns in NTRL as well as in FULL (Figures 2b and 2c) compare quite favorably with the trend pattern drawn from the observations (Figure 2a). In the ANTH simulations, on the other hand, the indirect effect of anthropogenic aerosols introduces cooling trends in the North America and the Northern Atlantic (Figure 2d), where the observed warming was largest in this period (1900–1949) (Figure 2a). The trend pattern in GHG (Figure 2e) looks less similar to the trends in the observations than do the trends in NTRL.

[9] To clarify the relative importance of the effect of WMGHGs and natural influences on the warming in the early 20th century, an optimal detection method using total least squares regression (TLS) [*Allen and Stott, 2003*] was applied to the simulated and observed SAT. In contrast to ordinary least squares regression (OLS), as was used in many previous studies (e.g., T02), TLS takes into account sampling uncertainty in the model responses when estimating the signal amplitudes, and gives an unbiased regression coefficient. Similar to the analysis of T02, we regress the observed spatio-temporal variations onto the three model-derived response patterns from GHG, ANTH, and NTRL to estimate the signal amplitudes for GHG, ANTH-GHG (i.e., the temperature response to all the anthropogenic influences except WMGHGs) and NTRL effects. The signal amplitude for ANTH-GHG is computed via a linear transformation from the GHG and ANTH responses (see T02 for more

details). Following the approach of *Stott et al.* [2001] the observed and simulated SATs in the early 20th century (1900–1949) were averaged decadally, expressed as anomalies with respect to the same period, and filtered by projecting onto T4 spherical harmonics. We calculate the signal amplitudes by estimating covariance matrices, for optimization, from intra-ensemble spread of the ensembles using a truncation of 10 EOFs. Applying the residual test of *Allen and Tett* [1999], we found that the residual in the regression was consistent with control variability. The uncertainty on the amplitudes was estimated from our 1300-year control simulation.

[10] The estimated signal amplitudes and uncertainty ranges (Figure 3a) indicate that, unlike with T02, only the natural contribution is detectable (i.e., only the uncertainty range for NTRL is entirely positive), and since the uncertainty range includes unity, the signal amplitude is consistent with the amplitude of the signal in observations. It should also be noted that the detection of the NTRL signal and its consistency with the observations is independent of the number of EOFs retained in the analysis (not shown). Therefore the detected natural contribution is robust. The two anthropogenic signals, on the other hand, have large uncertainty and are not detectable. Again this result is independent of number of EOFs retained in the analysis (not shown). To make a direct comparison with the analysis of T02, we repeated our analysis using OLS. We found that the best-estimated signal amplitudes are not largely different from those shown in Figure 3a (calculated with TLS). However, since OLS assume no sampling uncertainty in the model responses, the estimated uncertainty limits are smaller with OLS than those with TLS (not shown). It should be noted that, unlike with T02, the two anthropogenic signals have large uncertainty and are not detected even in our OLS analysis.

[11] Figure 3c shows best-estimated linear trend for the early half of the century. The total trend shows much better agreement with the observations than that in T02. Note that the best-estimated trends in Figure 3c are also not largely different from those with OLS. The natural forcing causes a warming trend of  $\sim 0.6\text{K/century}$ , which is about one half of the observed trend. This is consistent with the global annual mean SAT anomalies simulated in NTRL (Figure 1). The residual of the observed trend ( $\sim 0.4\text{K/century}$ ) may be caused by the combined anthropogenic forcings, primarily by the WMGHGs. However, the two anthropogenic signals are highly uncertain and are not detected. Therefore the cause of the residual trend is not obvious.

[12] The robustness of the NTRL signal is tested by regressing the observations onto the two simulated responses from ANTH and NTRL (Figures 3b and 3d). Again, only the natural contribution is detected while the net anthropogenic signal is highly uncertain and is not detected. This confirms the significance of the natural contributions to the early 20th century warming.

#### 4. Concluding Remarks

[13] Surface air temperature changes simulated by a global coupled climate model with different external forcings are investigated to detect the observed climate change signals in the early 20th century. Unlike with several

previous studies, the natural contribution is robustly detected in the observed early-century warming by investigating linear temperature trend patterns and by employing a regression-based optimal detection technique. Further investigation is needed to clarify the relative importance between a recovery from heavy volcanic eruptions and an increase in solar irradiance; the results of such a study will be reported elsewhere.

[14] In our statistical analysis, we cannot detect any anthropogenic contribution to the early 20th century warming. However, we do note that the uncertainty range of the greenhouse-gas contribution is consistent with the estimated range of observed warming; therefore we cannot rule out that anthropogenic factors, particularly WMGHGs have influenced global temperatures over the early 20th century.

[15] We should note that, since the uncertainty limits obtained from the optimal fingerprinting analysis is estimated using the control variability, our results are dependent on whether the control run correctly simulates observed multi-decadal internal climate variability. Our simple analysis shows that multi-decadal control variability of MIROC is comparable to the estimated observed variability, suggesting that our results using the optimal detection methodology are robust.

[16] In our simulations, all the known major external forcing factors are introduced in order to reduce the uncertainties that arise due to missing forcing agents, although we recognize there could be large uncertainties in the newly introduced forcing agents such as the historical emission of the carbonaceous aerosols. Nevertheless, the FULL ensemble shows quite similar spatio-temporal variations to the observations, suggesting that the errors in the external forcings are not obviously apparent.

[17] **Acknowledgments.** The authors thank the K-1 project members for their support and discussion, and two anonymous reviewers for their valuable comments. This work was supported by the Research Revolution 2002 (RR2002) of the Ministry of Education, Culture, Sports, Science and Technology, and by the Global Environment Research Fund (GERF) of the Ministry of the Environment of Japan. The Earth Simulator and a NEC SX-6 at NIES were employed to perform the CGCM simulations. The GFD-DENNOU Library was used for the figures.

## References

- Allen, M. R., and P. A. Stott (2003), Estimating signal amplitudes in optimal fingerprinting, part I: Theory, *Clim. Dyn.*, *21*, 477–491.
- Allen, M. R., and S. F. B. Tett (1999), Checking for model consistency in optimal fingerprinting, *Clim. Dyn.*, *15*, 419–434.
- Broccoli, A. J., K. W. Dixon, T. L. Delworth, T. R. Knutson, and R. J. Stouffer (2003), Twentieth-century temperature and precipitation trends in ensemble climate simulations including natural and anthropogenic forcing, *J. Geophys. Res.*, *108*(D24), 4798, doi:10.1029/2003JD003812.
- Delworth, T. L., and T. R. Knutson (2000), Simulation of early 20th century global warming, *Science*, *287*, 2246–2250.
- Hasselmann, K. (1997), Optimal fingerprints for the detection of time dependent climate change, *J. Clim.*, *6*, 1957–1971.
- Hasumi, H., and S. Emori (Eds.) (2004), K-1 coupled GCM (MIROC) description, *K-1 Tech. Rep. 1*, 34 pp., Cent. for Clim. Syst. Res., Univ. of Tokyo, Tokyo.
- Hegerl, G. C., T. J. Crowley, S. K. Baum, K.-Y. Kim, and W. T. Hyde (2003), Detection of volcanic, solar and greenhouse gas signals in paleoreconstructions of Northern Hemispheric temperature, *Geophys. Res. Lett.*, *30*(5), 1242, doi:10.1029/2002GL016635.
- Hirabayashi, Y., S. Kanae, I. Struthers, and T. Oki (2005), A 100-year (1901–2000) global retrospective estimation of the terrestrial water cycle, *J. Geophys. Res.*, *110*, D19101, doi:10.1029/2004JD005492.
- Johns, T. C., et al. (2003), Anthropogenic climate change for 1860 to 2100 simulated with the HadCM3 model under updated emissions scenarios, *Clim. Dyn.*, *20*, 583–612.
- Jones, P. D., and A. Moberg (2003), Hemispheric and large-scale surface air temperature variations: An extensive revision and an update to 2001, *J. Clim.*, *16*, 206–223.
- Lean, J., J. Beer, and R. Bradley (1995), Reconstruction of solar irradiance since 1610: Implications for climate change, *Geophys. Res. Lett.*, *22*, 3195–3198.
- Lefohn, A. S., J. D. Husar, and R. B. Husar (1999), Estimating historical anthropogenic global sulfur emission patterns for the period 1850–1990, *Atmos. Environ.*, *33*, 3435–3444.
- Meehl, G. A., W. M. Washington, C. M. Ammann, J. M. Arblaster, T. M. L. Wigley, and C. Tebaldi (2004), Combinations of natural and anthropogenic forcings in 20th century climate, *J. Clim.*, *17*, 3721–3727.
- Mitchell, J. F. B., et al. (2001), Detection of climate change and attribution of causes, in *Climate Change 2001: The Scientific Basis*, edited by J. T. Houghton et al., pp. 695–738, Cambridge Univ. Press, New York.
- Nakajima, T., M. Tsukamoto, Y. Tushima, A. Numaguti, and T. Kimura (2000), Modeling of the radiative process in an atmospheric general circulation model, *Appl. Opt.*, *39*, 4869–4878.
- Randel, W. J., and F. Wu (1999), A stratospheric ozone trends data set for global modeling studies, *Geophys. Res. Lett.*, *26*, 3089–3092.
- Sato, M., J. E. Hansen, M. P. McCormick, and J. B. Pollack (1993), Stratospheric aerosol optical depths, 1850–1990, *J. Geophys. Res.*, *98*, 22,987–22,994.
- Stott, P. A., S. F. B. Tett, G. S. Jones, M. R. Allen, J. F. B. Mitchell, and G. J. Jenkins (2000), External control of 20th century temperature by natural and anthropogenic forcings, *Science*, *290*, 2133–2137.
- Stott, P. A., S. F. B. Tett, G. S. Jones, M. R. Allen, W. J. Ingram, and J. F. B. Mitchell (2001), Attribution of twentieth century temperature change to natural and anthropogenic causes, *Clim. Dyn.*, *17*, 1–21.
- Sudo, K., M. Takahashi, J. Kurokawa, and H. Akimoto (2002), CHASER: A global chemical model of the troposphere: 1. Model description, *J. Geophys. Res.*, *107*(D17), 4339, doi:10.1029/2001JD001113.
- Takemura, T., T. Nakajima, O. Dubovik, B. N. Holben, and S. Kinne (2002), Single-scattering albedo and radiative forcing of various aerosol species with a global three-dimensional model, *J. Clim.*, *15*, 333–352.
- Tett, S. F. B., P. A. Stott, M. R. Allen, W. J. Ingram, and J. F. B. Mitchell (1999), Causes of twentieth-century temperature change near the Earth's surface, *Nature*, *399*, 569–572.
- Tett, S. F. B., et al. (2002), Estimation of natural and anthropogenic contributions to twentieth century temperature change, *J. Geophys. Res.*, *107*(D16), 4306, doi:10.1029/2000JD000028.

S. A. Crooks, Department of Physics, University of Oxford, Oxford OX1 3PU, UK.

T. Nagashima, T. Nozawa, and H. Shioyama, National Institute for Environmental Studies, Tsukuba, Ibaraki 305-8506, Japan. (nozawa@nies.go.jp)